Observations of Stimulated-Brillouin Scattering Initiated by Ponderomotive Force Density Fluctuations

H. E. Huey, A. Mase,[a] N. C. Luhmann, Jr.
University of California, Los Angeles, California 90024

and

W. F. DiVergilio and J. J. Thomson
TRW, Redondo Beach, California 90278

(Received 6 August 1979; revised manuscript received 2 June 1980)

This Letter reports the first observations of stimulated Brillouin scattering in microwave interaction with a plasma, as verified by the satisfaction of the frequency- and wavelength-matching rules and growth rate. A small amount of chamber reflectivity causes ion fluctuations due to the standing-wave ponderomotive force, which then serve as an enhanced noise level for the initiation of the instability.

PACS numbers: 52.25.Ps, 52.40.Mj

Stimulated Brillouin scattering (SBS) in a plasma is due to the interaction of an electromagnetic wave and an ion acoustic wave. The resultant wave may be scattered at various angles, but the scattering maximizes in the backward direction, with a characteristic frequency downshift of the ion acoustic frequency, $\omega_s = kc_s$, where c_s is the ion sound speed and k is given by momentum considerations as $2k_0$, where k_0 is the incident wave number. This process is important in laser fusion, since the scattered energy is not available to the compression process. SBS has been observed in laser-plasma interactions,[1,2] identified by the characteristic ω_s frequency shift. Here we report the first observations of SBS in microwave interaction with plasma, finding not only the frequency downshift in the reflected wave, but directly measuring the wavelength of the ion acoustic fluctuations. An interesting feature of these experiments is that a small chamber reflectivity sets up ion fluctuations which then serve as an enhanced noise level for the initiation of the stimulated Brillouin-scattered wave. After an initial fast growth time, we find the SBS reflectivity growth rate to agree with the classical calculations.[2]

The experiments were performed in an unmagnetized plasma of 75 cm diameter and 200 cm length, produced by a multifilament dc discharge with surface multidipole confinement. Typical operating parameters were gas filling pressure $(1-3)\times 10^{-4}$ Torr, electron density $n_e = 10^{10}-10^{11}$ cm^{-3}, electron temperature $T_e \simeq 2$ eV and electron-ion temperature ratio $T_e/T_i = 10-12$. Various gases were used including hydrogen, helium, neon, and argon. Experiments were performed at a number of microwave pump frequencies in the range 3–16 GHz, with peak powers up to 1 MW and pulse widths, τ_p, from 0.1–20 μs. The wave was launched along the chamber axis by a high-gain ($\simeq$20 dB) gridded horn, the radiation pattern of which gave an effective interaction length of 70–120 cm. In order to avoid possible complications introduced by effects other than SBS, e.g., the parametric decay instability, the electron density was adjusted to 0.1 of the critical density, n_c, for all experiments.

The incident and backscattered electromagnetic waves were separated for detection with use of either a circulator or directional coupler, and fed into a square law detector for power measurements or a spectrum analyzer for frequency-shift measurements. Ion waves were detected with movable Langmuir probes, after the microwave pump is off, thus avoiding the problem of rf pickup.

Since $T_e/T_i \gg 1$, Landau damping is rather small, and comparable to the damping due to ion collisions with the neutral background. From the discussion of Forslund, Kindel, and Lindman,[3] after a time sufficiently long that a scattered wave has time to traverse the system, one must solve the spatial scattering problem. The growth rate is then

$$\gamma_s = 2\gamma_0\left(\frac{c_s}{c}\right)^{1/2} = \omega_0\frac{c_s}{c}\left(\frac{n_e}{n_c}\frac{v_0^2}{v_e^2}\right)^{1/2}, \qquad (1)$$

where v_0 (v_e) is the oscillating (electron thermal) velocity and γ_0 is the maximum growth rate for the temporal problem. Comparing γ_s to the ion damping rate, we obtain the threshold condition.

Convincing evidence for the existence of the SBS above this threshold was obtained by verifying the frequency and wave vector rules: $\omega_0 = \omega$

$+\omega_s$, $\vec{k}_0 = \vec{k} + \vec{k}_s$ ($\omega, \vec{k}$ refer to the scattered wave). We found that the $\vec{k}$ selection rule was well satisfied for a variety of incident wave numbers and ion species. Figure 1 shows representative frequency spectra of the incident and reflected waves. Here the plasma was predominantly H_3^+, and the pulse length was 20 μs ($\omega_s \tau_p \cong 25$). The red-shifted component of the reflected wave appears when the incident power exceeds threshold. For all ion species and pump wavelengths the measured red shift was found to be in excellent agreement with the appropriate acoustic frequency. The measured threshold power agrees with the theoretical prediction and is obtained by setting γ_s equal to the measured ion wave damping rate ($\simeq 5 \times 10^4$ s^{-1}).

For typical experimental conditions, $c_s/c = 3 \times 10^{-5}$, $v_0/v_e = 0.5$, $n/n_c = 0.1$, and $\omega_0 = 2 \times 10^{10}$ s^{-1}, Eq. (1) predicts a growth time $\tau_g = \gamma_s^{-1} = 7.2$ μs. In the usual theory of SBS, ion acoustic fluctuations are assumed to grow from a small noise level. From the measured noise level and frequency spectrum in our plasma, and the above growth time, we would expect the SBS-driven ion waves to attain an amplitude $\delta n/n = 1\%$ approximately 50 μs after pump turnon. However, in these experiments, ion fluctuations at ω_s were observed to grow in a very short time, $\simeq \omega_s^{-1}$, to a level of a percent or so, and then to continue growing at the much lower rate predicted by Eq. (1). This unexpected behavior may be explained

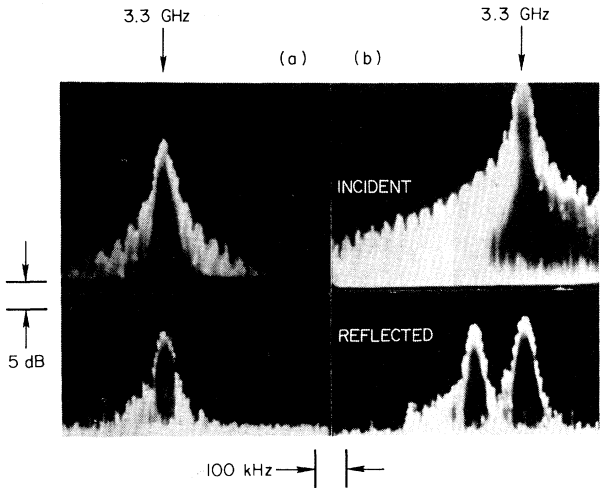

FIG. 1. Spectrum analyzer traces of incident and reflected microwave signals of both (a) below and (b) above threshold for SBS. The red shift corresponds to the measured ion wave frequency and to the predicted frequency for the predominantly H_3^+ plasma. (a) $P_0 = 60$ kW, $v_0/v_e \simeq 0.31$; (b) $P_0 = 250$ kW, $v_0/v_e \simeq 0.63$.

by taking into account the small, but finite, amount of power reflected from the chamber end wall ($\simeq 1\%$), which sets up a standing electromagnetic wave.

It is perhaps surprising that such a small amount of reflectivity can produce significant ripples in the standing-wave power. To see this, consider the power–standing-wave ratio

$$(E_{\max}/E_{\min})^2 = (1 + r^{1/2})^2/(1 - r^{1/2})^2, \tag{2}$$

where r is the chamber reflectivity. For $r = 1\%$, $(E_{\max}/E_{\min})^2 = 1.5$. The ponderomotive force associated with the electric-field pressure gradient drives ion-density fluctuations. We will calculate these fluctuations and show that there is a component that directly couples with the SBS-backscattered wave.

We express the forward and reflected waves as

$$E_i = E_0 \sin(\omega_0 t - k_0 x) \tag{3}$$

and

$$E_r = r^{1/2} E_0 \sin(\omega_0 t + k_0 x), \tag{4}$$

respectively. The ion acoustic wave equation is

$$\frac{\partial^2 \tilde{n}}{\partial t^2} - c_s^2 \frac{\partial^2 \tilde{n}}{\partial x^2} = 4 k_0^2 c_s^2 n_0 r^{1/2} \frac{v_0^2}{v_e^2} \cos 2k_0 x, \tag{5}$$

where $\tilde{n}$ is the fluctuating ion density. The right-hand side is the ponderomotive source term. The solution of Eq. (5) is

$$\tilde{n}/n_0 = r^{1/2} (v_0/v_e)^2 \cos(2k_0 x)(1 - \cos \omega_s t). \tag{6}$$

This consists of a zero-frequency component and two traveling waves. The zero-frequency mode scatters the incoming wave in the manner of a grid (i.e., Bragg scattering) while the Thomson scattering from the traveling waves results in both red- and blue-shifted components to the backscattered radiation.

The backscattered wave equation is

$$\left(\frac{\partial^2}{\partial t^2} + \omega_{pe}^2 - c^2 \frac{\partial^2}{\partial x^2} \right) E_s = \omega_{pe}^2 \frac{\tilde{n}}{2n_0} E_0 \sin(\omega_0 - k_0 x). \tag{7}$$

For the backscattered red-shifted wave, which satisfies the frequency- and wave-number–matching conditions for SBS, Eq. (7) becomes

$$2\omega_0 c \frac{\partial E_s}{\partial x} = -\frac{\omega_{pe}^2}{2} r^{1/2} \frac{v_0^2}{v_e^2} E_0. \tag{8}$$

With the chamber end-wall boundary condition $E_s(L) = 0$, the solution is

$$E_s = \left(\frac{\omega_{pe}}{2\omega_0} \right)^2 r^{1/2} \frac{v_0^2}{v_e^2} E_0 k_0 (L - x). \tag{9}$$

The ponderomotive-force–driven density fluctuations of Eq. (6) and the resultant scattered wave predicted by Eq. (9) occur on the time scale ω_s^{-1}. For longer times, we expect continued growth due to the usual SBS mechanism.

Figure 2(a) shows the normalized density fluctuation level $\tilde{n}/n_0$ observed at a fixed position as a function of time. The ponderomotive-force–driven fluctuations are clearly visible in the low-power He case, where the pump power was below threshold for SBS. In contrast, at powers well above threshold, as seen in the H example, the slowly growing SBS fluctuations are superposed on the ponderomotive-force–driven fluctuations. Concurrent analysis of the backscattered electromagnetic wave also shows the slow growth of the red-shifted component. It should be noted that the predicted Thomson-scattered blue-shifted component was also observed, with amplitude always more than 10–20 dB below that of the red-shifted component.

Equation (6) also predicts that the peak fluctuation level at the first turning point ($\omega_s t_p = \pi$) is given by

$$\tilde{n}(t_p)/n_0 = 2r^{1/2}(v_0/v_e)^2 . \qquad (10)$$

In the inset to Fig. 2(a), t_p is plotted as a function of ω_s, which is varied by using different ion species showing good agreement with theory. Figure 2(b) shows $\tilde{n}(t_p)/n_0$ vs v_0^2/v_e^2. The best fit is obtained for $r = 0.6\%$, which is consistent with our estimates of 1% obtained from Eq. (9) and the measured power reflected back into the horn. This level of agreement is consistent with our uncertainties in quantities such as $(v_0/v_e)^2$ and interaction length. We have also done experiments with a reflectivity of $\approx 5\%$ and found the scaling of Eqs. (9) and (10) to be valid.

The measured growth time of the backscattered wave, after the initial ponderomotive-force–driven response, is shown in Fig. 3 as a function of v_0/v_e, for a hydrogen plasma. The agreement with the prediction of Eq. (1) (solid curve) is seen to be excellent. We have run some experiments with $v_0/v_e > 1$ and observed significantly faster growth rates than those predicted by Eq. (1). The cause of this discrepancy is currently under investigation.

It should be noted that the model described here will not be valid for time scales much greater than the ion wave damping time. On these time scales, the traveling-wave portion of the ponderomotive-force response will damp away and no longer act as an enhanced noise level for SBS.[4]

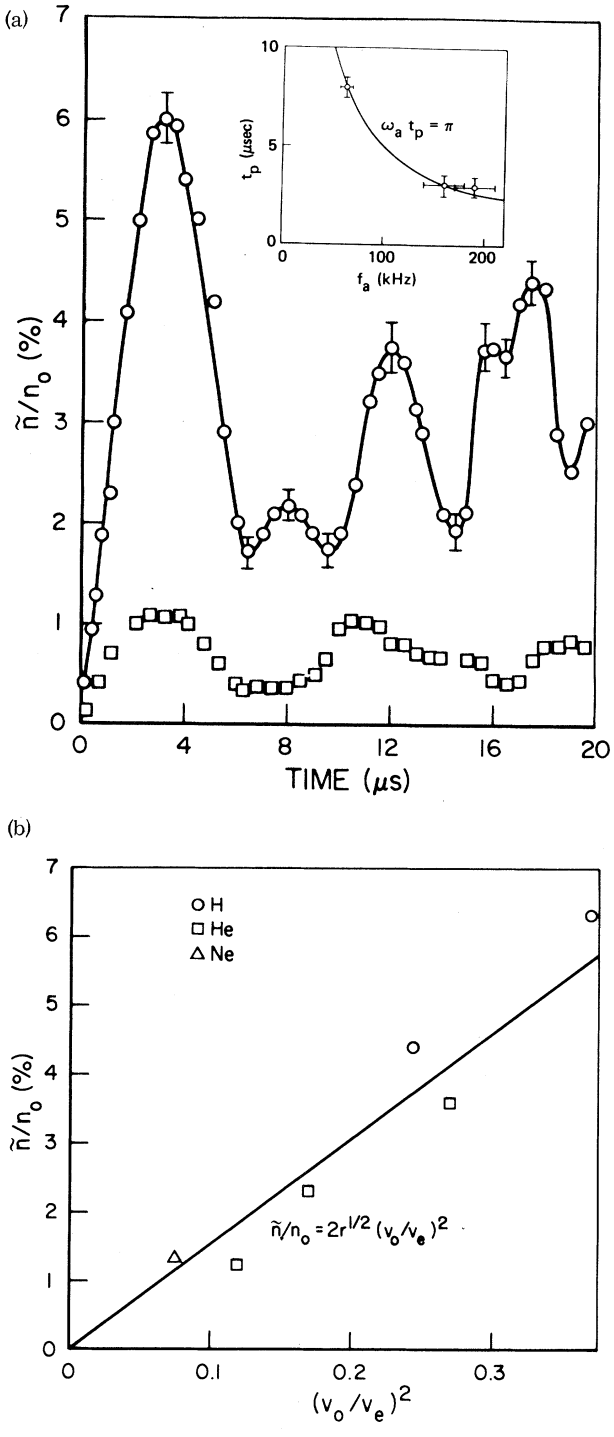

FIG. 2. (a) Normalized density fluctuation level $\tilde{n}/n_0$ as a function of time. The squares correspond to a helium plasma ($v_0/v_e \simeq 0.37$) while the circles correspond to hydrogen ($v_0/v_e \simeq 0.68$). The inset shows the measured t_p vs f_s together with the predicted $\omega_s t_p = \pi$ curve. (b) Measured $\tilde{n}(t_p)/n_0$ vs $(v_0/v_e)^2$ together with predicted $\tilde{n}/n_0 = 2r^{1/2}(v_0/v_e)^2$ curve.

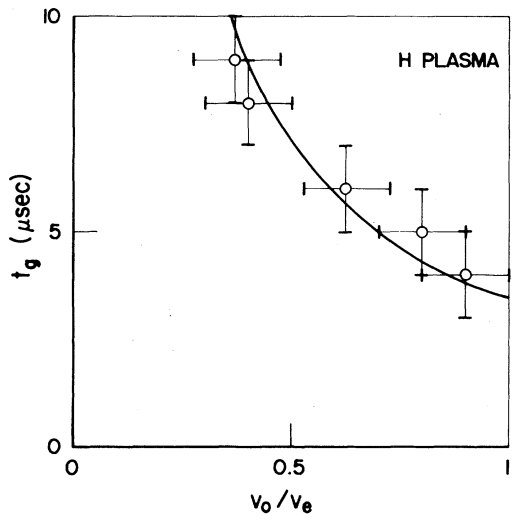

FIG. 3. Measured growth rate as a function of v_0/v_e compared with theory.

In addition, increased Landau damping due to ion heating may be important. Simulations of these experiments have been performed using a wave-optics–hydrodynamics code.[4] Good agreement with these results were found, including the magnitude of the red-shifted component (Fig. 1) and the detailed time history of the ion wave [Fig. 2(a)]. A more thorough discussion, including long-time effects is forthcoming.

In conclusion, for the first time in microwave plasma interaction, we have observed the stimulated–Brillouin-scattering instability. The time evolution of the ion fluctuations and reflected electromagnetic radiation are in good agreement with the predictions of an analytic calculation employing a spatially dependent ponderomotive force, giving rise to an enhanced SBS initiation level. In a laser fusion experiment, reflection from the critical surface will play the role that chamber reflectivity played in this experiment. The resultant enhanced noise level may lead to higher levels of reflectivity.

We will discuss in a future publication SBS saturation levels and the effect of finite bandwidth.

We would like to acknowledge fruitful discussions with Dr. C. J. Randall and Dr. D. W. Forslund. This work was supported in part by the U. S. Department of Energy under Contracts No. DE-AC08079DP400116 and No. DE-AS03-76-SF00034 and in part by the U. S. Air Force Office of Scientific Research Contract No. F490620-76-0012.

---

[a]Permanent address: Faculty of Engineering, Nagoya University, Nagoya 464, Japan.

[1]B. H. Ripin, F. C. Young, J. A. Stamper, C. M. Armstrong, R. Decoste, E. McLean, and S. E. Bodner, Phys. Rev. Lett. 29, 611 (1977).

[2]D. W. Phillion, W. L. Kruer, and V. C. Rupert, Phys. Rev. Lett. 39, 1529 (1977).

[3]D. W. Forslund, J. M. Kindel, and E. L. Lindman, Phys. Fluids 18, 1002 (1975).

[4]C. J. Randall, to be published.

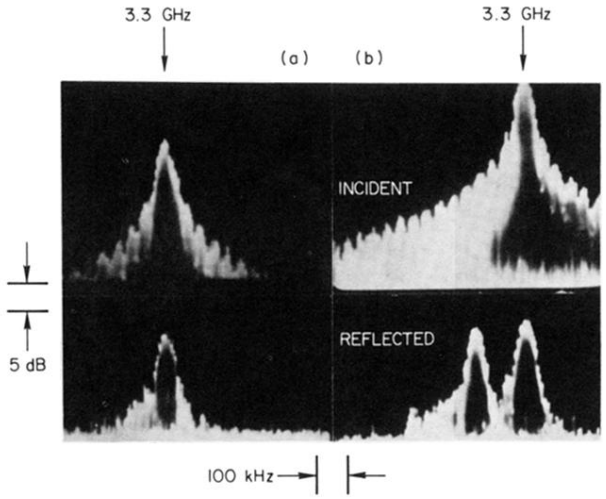

FIG. 1. Spectrum analyzer traces of incident and reflected microwave signals of both (a) below and (b) above threshold for SBS. The red shift corresponds to the measured ion wave frequency and to the predicted frequency for the predominantly H_3^+ plasma. (a) P_0 = 60 kW, $v_0/v_e \simeq 0.31$; (b) P_0 = 250 kW, $v_0/v_e \simeq 0.63$.